A New Modeling and Experimental Framework to Characterize Hindered and Restricted Water Diffusion in Brain White Matter

Y. Assaf[1,2], R. Z. Freidlin[3], G. K. Rohde[4], P. J. Basser[4]

[1]Tel Aviv Sourasky Medical Center, Tel Aviv, Israel, [2]Tel Aviv University, Tel Aviv, Israel, [3]Center for Information Technology, The National Institutes of Health, Bethesda, Maryland, United States, [4]National Institute of Child Health and Human Development, The National Institutes of Health, Bethesda, Maryland, United States

Introduction

White matter is composed of ordered fascicles whose axons are surrounded by a complex extra-axonal environment containing astrocytes, glia and extracellular matrix. It is suggested that the diffusion weighted (DW) signal at low and high b values may probe different water pools. Recently, a model of water diffusion in white matter was proposed (1) that contains a hindered extra-axonal compartment, whose diffusion properties are characterized by an effective diffusion tensor, and an intra-axonal compartment, whose diffusion properties are characterized by a restricted model of diffusion within cylinders. Here, we have used this model to fit experimental data collected from areas of crossing white matter fibers.

Theoretical Background

The most general form of the model (Eq. [1]) defines the net signal decay, $E(\mathbf{q},\Delta)$, as a sum of signals from the hindered ($E_h(\mathbf{q},\Delta)$) and restricted ($E_r(\mathbf{q},\Delta)$) compartments, and f_h and f_r are the T_2-weighted population fractions of the hindered and restricted compartments. Because exchange between the two compartments should be extremely slow in relation to the experimental time scale, we use the "slow exchange" limit. While diffusion in the hindered compartment is explained by an effective diffusion tensor, for which the mathematical description has already been developed (2), the mathematical description of the restricted component is more challenging. One important simplification we propose is that the signal decay in the restricted compartment can be decomposed into contributions arising from spins diffusing parallel and perpendicular to the axon's axis. This simplifies the mathematical description of the restricted component as diffusion parallel to the fibers can be treated as one-dimensional free diffusion (Stejskal-Tanner relation) while diffusion perpendicular to the fibers can be described as restricted diffusion within impermeable cylinders. In clinical DWI applications the diffusion gradient waveform is approximately constant. In these cases, we can use an asymptotic form of $E_\perp(\mathbf{q}_\perp,\Delta)$ for a restricted cylinder proposed by Neuman (3) under the assumption of a constant field gradient (Eq. [2]) to describe the signal decay perpendicular to fibers in the restricted component.

$$[1]\quad E(\mathbf{q},\Delta)=\sum_{i=1}^{M} f_h^i \cdot E_h^i(\mathbf{q},\Delta)+\sum_{j=1}^{N} f_r^j \cdot E_r^j(\mathbf{q},\Delta)$$

$$[2]\quad E_\perp(\mathbf{q}_\perp,2\tau)=e^{-\frac{4\pi^2R^4|\mathbf{q}_\perp|^2}{D_\perp\tau}\frac{7}{296}\left(2-\frac{99}{112}\frac{R^2}{D_\perp\tau}\right)}$$

Methods

Excised spinal cords were scanned on a 7T spectrometer. Two sections of a freshly excised cervical pig spinal cord were placed in an apparatus shown in Figure 1. Diffusion experiments were performed using a PGSE sequence with the following parameters: TR/TE= 2000/200ms, Δ/δ=150/40ms. The field of view (FOV) was 5cm, matrix size was 32 x 32 and slice thickness was 15mm. Pulsed gradients were incremented from 0 to 5.25 G/cm in 16 steps and measured in 31 non-collinear gradient directions.

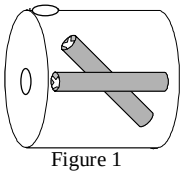

Figure 1

The model presented in Eq. [1] was used to estimate microstructural parameters from diffusion data using a non-linear regression routine. Four combinations of compartmental configurations were used: (1) 1 hindered and 0 restricted compartments were used to fit a single fiber data at low b values (standard diffusion tensor analysis). (2) 1 hindered and 1 restricted compartment was used to fit a single fiber data including high b values. (3) 2 hindered and 0 restricted compartments were used to fit two crossing fibers data at low b values. (4) 1 hindered and 2 restricted compartments were used to fit data where fibers crossed including the high b value data. Extracted parameters included the population fractions of the hindered and restricted multiple compartments, the eigenvectors and eigenvalues of the hindered part (DTI), as well as $D_{//}$ of the restricted part and the orientation of the restricted part in spherical coordinates. The noise floor, η, was also estimated in each fit. Once parameters were estimated, we resampled $E(\mathbf{q})$ on a uniform grid in q-space and obtained the 3-D FFT, which corresponds to the 3-D average propagator, $p(\mathbf{r})$. The 3-D FFT matrices were then used to produce iso-probability surface plots shown in Figures 2 and 3.

Results

The diffusion tensor model (one hindered component only) gave accurate results in areas where there was a single fiber bundle (Figure 2). In areas of crossing fibers, the diffusion tensor model provided the mean orientations of the two fiber bundles. The double tensor model, that *a priori* has the chance of separating two-fiber orientations, failed to detect the two fiber populations in the low b-value range. Only in 3 out of 33 pixels in the crossing fiber bundle area did the double tensor model give reasonable results (data not shown). For the 1 hindered and 1 restricted model there was an almost a one to one correspondence between the orientations of the hindered and restricted fiber orientations that were computed in areas of single bundle of neuronal fibers (Figure 3). The other extracted parameters (diffusion eigenvalues) were typical of dead neuronal tissue. In regions of crossing fibers we also tested the combination of two restricted and one hindered compartments. Indeed this model was able to separate two distinct fiber bundles within the crossing fiber area with extracted orientations only slightly different from the true values (ϕ and φ of 73 ± 22^0 and 44 ± 11^0 for the 45^0 fiber, and of 83 ± 6^0 and 104 ± 4^0 for the 90^0 fiber.

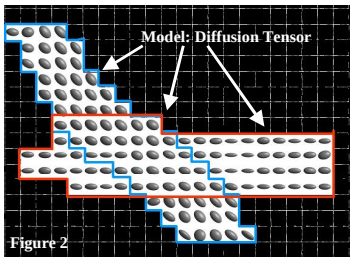

Figure 2

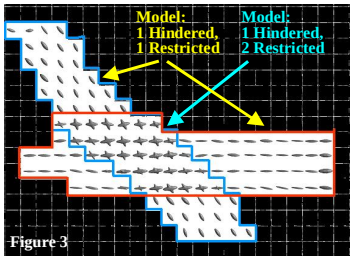

Figure 3

Discussion

The success of the 1 hindered and 1 restricted compartment model whose principal axes are aligned with each other in describing coherent nerve pathways, suggests that one can use DTI-based methods to track fibers reliably in this case. However, in regions with two or more distinct fiber orientations, the effective diffusion tensor represents only a powder average of the diffusion tensors from the various hindered compartments. By contrast to DTI, powder averaging does not take place in multiple restricted compartments. The contribution of each can be superposed since the motion within each fiber is independent of the other. Using the spinal cord phantom, we were able to show that the restricted model can distinguish between fibers crossing at 45° with reasonable accuracy. The model itself also provides other parameters such the principal diffusivities for the various compartments and the population fractions. Microstructural information from the restricted compartment(s) might have great utility in certain clinical pathologies, e.g., multiple sclerosis, and in some subtle white matter disorders.

Conclusions

We propose a model of water diffusion in white matter having hindered diffusion in the extra-axonal compartment and restricted diffusion in the intra-axonal compartment. From experimental $E(\mathbf{q})$ data, microstructual parameters (e.g., $D_{//}$, $\lambda_{//}$, $\lambda_\perp$) can be estimated. From the best fit to $E(\mathbf{q})$ data, a 3-D displacement probability distribution, $p(\mathbf{r})$, can be calculated. The determination of the orientation(s) of the restricted compartment(s) should provide improved angular resolution and fiber direction(s), which should aid tractography studies. It is expected that this combined theoretical and experimental framework should provide new microstructural parameters that will allow us to follow subtle changes occurring in white matter in disease, development, aging and degeneration with greater specificity and selectivity.

References

(1) Assaf Y, Basser PJ. Proc. Soc. Magn. Reson. Med. 11, 588, **2003**. (2) Basser PJ, Mattiello J, Le Bihan D. Biophys. J. 66, 259, **1994**. (3) Neuman CH. J. Chem. Phys. 60, 4508, **1974**.